

ApJ, submitted May 7, 2019

AGN Environments in the Sloan Digital Sky Survey I: Dependence on Luminosity, Type, and M_{BH}

Natalie E. Strand

Department of Physics, University of Illinois at Urbana-Champaign

Urbana, IL 61801

nstrand@uiuc.edu

and

Robert J. Brunner, Adam D. Myers

Department of Astronomy, University of Illinois at Urbana-Champaign

Urbana, IL 61801

ABSTRACT

We explore how the local environment is related to the type and luminosity of AGN. Recent simulations and observations are converging on the view that the extreme luminosity of quasars is fueled in major mergers of gas-rich galaxies. In such a picture, quasars are expected to be located in regions with higher density of galaxies where mergers are more likely to take place. However, in this picture, the activity observed in low-luminosity AGN is due to secular processes that are less dependent on the local galaxy density. To test this hypothesis, we compare the local photometric galaxy density around Type I quasars on kiloparsec scales to the local density around low-luminosity, narrow line AGN and Type II quasars. We find that the mean overdensity of photometric galaxies around the environment of low-luminosity AGN is ≈ 1.7 times less than the mean overdensity around Type I quasars with significance $> 3\sigma$, but the environment density of photometric galaxies around Type II quasars is not significantly different than the environment around Type I quasars. We also find that on scales $\lesssim 300 h_{70}^{-1}$ kpc, quasars with more massive black holes have an environment density 1.13 times ($> 3\sigma$) more than that of quasars with less massive black holes. It will be necessary for new merger models simulating the origin of quasars to explain why quasars with more massive black holes are formed in or ultimately end up in richer environments on scales $\lesssim 300 h_{70}^{-1}$ kpc.

Subject headings: cosmology: observations — large-scale structure of universe — quasars: general — surveys

1. INTRODUCTION

The local environments of quasars yield valuable insight into the formation history and evolution of AGN (e.g., Ellingson et al. 1991). Quasar environments were first studied by Bahcall, Schmidt, & Gunn (1969), who used a sample of five quasars to show that quasars are associated with galaxy clusters. Yee & Green (1984) found that quasars reside in regions with higher galaxy density, and more recent work has confirmed that quasars are found in regions of galaxy groups or clusters of poor to moderate richness (Bahcall & Chokshi 1991; Fisher et al. 1996; McLure & Dunlop 2001; Wold et al. 2001; Coldwell et al. 2002; Barr et al. 2003). Although studies of several X-ray- and radio-selected samples have found evidence for a relationship between environment and AGN activity (e.g., Wurtz et al. 1997; Best 2004; Söchting et al. 2004), the Sloan Digital Sky Survey (SDSS) is the first survey to allow meaningful studies of quasar environments, because it samples large numbers of both quasars and galaxies at $z \lesssim 0.4$. Using SDSS data, Serber et al. (2006) concluded that the over-density of photometric galaxies around quasars increases with decreasing angular scale, but is independent of redshift for $z \leq 0.4$. They also showed evidence for a higher density of galaxies around more luminous quasars at scales less than $100 h^{-1}$ kpc, while at larger angular scales, the density appears to be independent of luminosity (see also Porciani & Norberg 2006; da Angela et al. 2007; Myers et al. 2007a).

The results of Serber et al. (2006) agree with other studies showing enhanced clustering of quasars on small scales. Djorgovski (1991) first linked the excess of quasar clustering on small scales to galaxy interactions. Studies of small-scale clustering of quasars (e.g., binary and triplet quasars) also support the hypothesis that there is excess quasar clustering on scales of $\lesssim 100 h^{-1}$ kpc (Kochanek et al. 1999; Mortlock et al. 1999; Hennawi et al. 2006; Djorgovski et al. 2007; Myers et al. 2007a).

An excess of quasar pairs on small scales naturally follows from a merger origin for quasar activity, whether these pairs simply trace biased groups where mergers are likely to occur (Hopkins et al. 2007) or are being excited in merging galaxies (Djorgovski 1991; Myers et al. 2007b). Hopkins et al. (2006) have developed a unified, merger-driven framework that naturally predicts that quasar environments should be highly biased (Hopkins et al. 2007). These simulations show that major mergers between gas-rich galaxies are the likely mechanisms to trigger bright quasar activity, and that this activity is a phase in the evolution of massive spheroidal galaxies (Hopkins et al. 2005b, 2007). In contrast, secular mechanisms may

fuel the activity in most low-luminosity AGN, implying that the small-scale environments of these objects should have a smaller bias (Hopkins & Hernquist 2006; Hopkins et al. 2007).

The merger view suggests that objects driven by major mergers will have biased environments on small scales, whereas objects fueled by secular means might be in less rich environments. Such a simplification hides many subtleties, however, as secular mechanisms such as harassment can probably only occur in slightly overdense environments. Further, for objects whose observed characteristics differ purely because of viewing angle or internal structure (Antonucci 1993; Elvis 2000), there should be no particular difference in local environment. This, of course, would only be the case if that structure is not correlated with fueling, as could occur, for instance, if more luminous quasars had strong winds. It is therefore important to better constrain quasar environments to understand what aspects of the types of AGN are explained by formation history, fueling, or simply by structure and orientation.

In this paper, we address this challenge by studying the nature of AGN environments. We improve upon the most recent SDSS study, Serber et al. (2006), in several ways. First, we use larger samples of quasars and galaxies and include cuts in photometric redshift space to eliminate interloping foreground or background objects. By using photometric redshift cuts, we obtain overdensity estimates with more realistic errors and are able to extend the study of AGN environments in the SDSS to $z \leq 0.6$. We compare the overdensity of quasars to the overdensity of other types of AGN, including low-luminosity, narrow-line AGN, and Type II quasars. Additionally, we investigate the relationship between the overdensity of a quasar’s local environment and its black hole mass. The data samples used in this paper are discussed in Section 2, and the technique for calculating overdensities is discussed in Section 3. Our results are presented in Section 4. Throughout the paper, we assume a concordance cosmology $\Omega_M = 0.3$, $\Omega_\Lambda = 0.7$, $H_0 = 70 \text{ km s}^{-1} \text{ Mpc}^{-1}$ (with $h = 0.7$) in order to compare to results from previous studies.

2. DATA

2.1. Spectroscopic Targets

The sample of spectroscopic quasar targets is taken from the Sloan Digital Sky Survey Fifth Data Release (DR5; Adelman-McCarthy et al. 2007). We draw our set of quasars from the DR5 Quasar Catalog (Schneider et al. 2007), which includes K -corrected absolute i -band magnitudes for each object. Following Serber et al. (2006), we restrict our quasar sample to have $-24.2 \leq M_i \leq -22.0$. We apply masks to eliminate objects within $2.0 h_{70}^{-1} \text{ Mpc}$ of the

survey edge or a masked area, which further reduces the sample to 3,279 quasar targets for $z \leq 0.4$ and 4,270 objects in the redshift range $0.4 \leq z \leq 0.6$. A subset of these quasars are matched to black hole mass estimates calculated using H_β emission line widths in the catalog produced by Shen et al. (2007, in preparation).

We use other AGN samples to test where quasars and AGN may fit into a merger-driven paradigm. We select a sample of objects classified as narrow-line AGN from Kauffmann et al. (2003)¹ and cut the original sample to match the low redshift limit of the main quasar sample ($z \geq 0.08$). After masking, the AGN target sample has 39,461 objects with $0.08 \leq z \leq 0.37$. We draw subsets of Type II quasar targets from the sample presented by Zakamska et al. (2003). After cutting the sample to match the high redshift limit of the main quasar sample ($z \leq 0.6$) and masking this sample as described above, we are left with 217 targets with $0.3 < z \leq 0.6$. Figure 1 shows the redshift distribution of the spectroscopic AGN samples used in this paper.

We compare the environments of our quasar targets to a sample of spectroscopic galaxies selected from the same area of the sky as the main quasar sample. The spectroscopic galaxy target sample consists of Primary SDSS DR5 objects spectroscopically classified as galaxies with $0.08 \leq z \leq 0.4$ and extinction-corrected magnitude of $i < 18.5$. We mask the spectroscopic galaxy sample in the same manner as the quasar targets and remove the 37,930 galaxies that are also in the AGN sample, resulting in a final sample of 221,036 spectroscopic galaxies. In order to calculate absolute magnitudes for the spectroscopic galaxies, we generate K -corrections using the method of Blanton et al. (2007). A subset of 33,752 L^* galaxies was selected by choosing galaxies within 0.25 magnitudes of the i -band L^* value of $M_i = -21.59$ (Blanton et al. 2003).

2.2. Photometric Galaxies

The environments of our spectroscopic targets are studied by counting photometric galaxies within $2.0 h_{70}^{-1}$ Mpc. The photometric galaxies are drawn from the SDSS DR5 database by selecting all primary objects photometrically classified as galaxies with r -band extinction corrected magnitude in the range $14.0 \leq r \leq 21.0$ ². All of these objects have been assigned photometric redshifts via a template-fitting technique as described in Csabai et al. (2003). Our final photometric galaxy sample of over 28 million (28,856,324) objects consists

¹<http://www.mpa-garching.mpg.de/SDSS/DR4/Data/agncatalogue.html>

²Note that Serber et al. (2006) used an r -band limit on their photometric galaxies rather than i -band as stated in their paper (W. Serber and R. Scranton, private communication).

of only those objects that pass the flag requirements for a clean galaxy sample³. Figure 1 shows the redshift distribution of our photometric galaxy.

3. TECHNIQUE

We count the number of photometric galaxies within a comoving radius of $2.0 h_{70}^{-1}$ Mpc for each spectroscopic target object (e.g., spectroscopic quasar, AGN, or spectroscopic galaxy), excluding any galaxies that are within $25 h_{70}^{-1}$ kpc of the target. At $z < 0.4$, $25 h_{70}^{-1}$ kpc corresponds to an angular size of $> 3.3''$, which is approximately twice the average seeing in DR5 (Adelman-McCarthy et al. 2007). At angular scales smaller than this, deblending hinders faint proximate galaxy detection. We use caution analyzing data at scales $< 30 - 50 h_{70}^{-1}$ kpc, because we extend beyond $z = 0.4$, which decreases the angular scale, and because bright quasars will raise nearby sky background values, further complicating detection of faint galaxies in the environment.

We generate a large number of random positions in the DR5 footprint area for each redshift increment of 0.001 in our redshift range of $0.08 \leq z \leq 0.6$. We mask the positions in same manner as we masked the spectroscopic targets, leaving at least 1,000 random positions that are more than $2.0 h_{70}^{-1}$ Mpc away from the survey edge or a masked area for each redshift value. We count the number of photometric galaxies within a designated comoving distance around random positions and calculate the mean number of counts for that redshift increment as

$$R_i = \frac{\sum_z R_z}{N_z} \quad (1)$$

where N_z is the number of random postions R_z at a given redshift increment z . We calculate the standard deviation on the mean as

$$e_{R_i}^2 = \frac{N_z}{N_z - 1} (\overline{R_i^2} - \overline{R_i}^2) \quad (2)$$

Spectroscopic target bincounts C_i are matched with the mean random bincounts (and standard deviation) at the redshift increment closest to the target's redshift R_i . We calculate a mean overdensity in a particular scale, redshift, or absolute magnitude bin δ_{bin} as

$$\delta_{bin} = \frac{\sum_i^N C_i}{\sum_i^N R_i} = \frac{C_{bin}}{R_{bin}} \quad (3)$$

³as defined by <http://cas.sdss.org/astro/en/help/docs/realquery.asp#flags>

where C_i is the counts around each target in the bin, R_i is the mean counts around random positions at the corresponding redshift, and there are N total targets in the bin. The error on the overdensity is given by

$$\left(\frac{e_{\delta_{bin}}}{\delta_{bin}}\right)^2 = \left(\frac{e_{C_{bin}}}{C_{bin}}\right)^2 + \left(\frac{e_{R_{bin}}}{R_{bin}}\right)^2 \quad (4)$$

where $e_{C_{bin}} = \sqrt{C_{bin}}$ and $e_{R_{bin}}^2 = \sum_i^N e_{R_i}^2$.

3.1. Comparison with Previous Techniques

To this point, our technique and results (as shown in Figures 2 and 3) are consistent with those of Serber et al. (2006). Figure 2 shows the mean overdensity of photometric galaxies around spectroscopic quasars as a function of redshift. Over the redshift range $0.08 \leq z \leq 0.4$, we see no obvious evolution of overdensity. Figure 3 shows the mean overdensity of photometric galaxies around spectroscopic quasars and spectroscopic galaxies as a function of absolute i -band magnitude. There is an increase of overdensity around spectroscopic galaxies as the galaxy absolute magnitudes increase. On the smallest scales, overdensity around spectroscopic quasars increases with absolute magnitude, but this trend becomes less pronounced on larger scales.

3.2. δz Cut

One of the difficulties in using photometric galaxy samples for overdensity measurements is the issue of projection effects, so we use photometric redshifts to minimize this complication. We apply a redshift cut on the photometric galaxies so that only those galaxies which satisfy $|z_{target} - z_{photogal}| \leq \delta z$ are counted in each bin. We verify that the projection effect issue is mitigated without introducing systematics by calculating overdensities for random positions with the same redshift distribution as the quasar sample. We find that the overdensities of photometric galaxies around random positions is consistent with zero on all scales with and without the photometric redshift cut. We use the value $\delta z = 0.05$, which is large enough to take the effective rms error of the photometric redshifts into account ($\Delta z_{rms} = 0.04$ for $r < 18$; Budavari et al. 2003), for all further analysis. We have tested other values for the photometric redshift cut and find that they give consistent results.

Table 1 shows the mean overdensity of photometric galaxies around quasars and spectroscopic L^* galaxies with and without the δz cut. The ratio of mean overdensities around

quasars to overdensities around L^* galaxies does not appreciably change when the δz cut is used. We see, however, that the errors on the mean overdensities with the δz cut have increased. We believe these larger errors are actually more realistic: with no δz cut, objects not actually correlated with the target will reduce Poissonian error estimates. We use the δz cut to extend our redshift range to include spectroscopic targets with $0.08 \leq z \leq 0.6$ without concern that foreground objects will contaminate the overdensity measurements.

Figure 4 shows the overdensity of photometric galaxies around quasars as a function of redshift including the δz cut. There is again no obvious evolution of overdensity over the redshift range $0.08 \leq z \leq 0.6$. The mean overdensity of photometric galaxies around spectroscopic quasars and spectroscopic galaxies as a function of absolute i -band magnitude including the δz cut is shown in Figure 5. All subsequent figures will include the $\delta z = 0.05$ cut.

4. RESULTS

We examine the relationship of overdensity with scale for quasars as a function of redshift in Figure 6. One clear trend is the decrease at the smallest scales. This artifact is likely due to the most luminous quasars biasing their local environment. This “glare” makes deblending objects difficult, as well as increasing the sky background so that the signal to noise of nearby faint galaxies is decreased below detection limits. For dimmer target objects, such as the Type II quasars, narrow-line AGN, and less luminous quasars, there is little or no glare effect.

By plotting the ratio of overdensities around $0.4 < z \leq 0.6$ quasars to the overdensity around $z \leq 0.4$ quasars in the lower panel of the figure, we obtain measures of their relative bias. Table 2 compares the cumulative overdensities at several scales of interest. There is some evolution with redshift of quasar clustering on small scales that was not obvious in Figure 4. At a scale $\approx 140 h_{70}^{-1}$ kpc (which corresponds to approximately $100 h^{-1}$ kpc when $h = 1.0$), the overdensity around the higher redshift quasars is ≈ 1.2 times the overdensity around the low redshift quasars with a significance $> 3\sigma$.

The top panel of Figure 7 shows the mean overdensity as a function of comoving scale for quasars in two luminosity bins, low-luminosity, narrow-line AGN, and Type II quasars. Here we see the glare effect more dramatically, especially for the brighter quasar sample. The middle panel of Figure 7 shows the ratio of Type II quasar overdensity to the overdensity of bright ($-24.2 \leq M_i < -23.3$) and dim ($-23.3 \leq M_i \leq -22.0$) quasars in the redshift range $0.3 \leq z \leq 0.6$. At scale $\approx 140 h_{70}^{-1}$ kpc, there is no significant difference between

the environment of Type II quasars and bright quasars (ratio of mean overdensities = 0.96, with significance 0.4σ). The ratio of AGN overdensity to the overdensity of bright and dim quasars in the range $0.08 \leq z \leq 0.37$ is shown in the lower panel of Figure 7. At scale $\approx 140 h_{70}^{-1}$ kpc, the environment of bright quasars is about 1.6 times more overdense than the environment of AGN with a significance $> 3\sigma$. The cumulative overdensities at several radii of interest are summarized in Table 3.

Figure 8 shows the relationship between overdensity and comoving scale as a function of black hole mass. At all scales, quasars with higher mass black holes are located in more overdense environments (significance $> 3\sigma$), which is consistent with the well-known relationship between black hole mass and dark matter halo mass, the so-called M - σ or $M_{\text{DMH}}\text{-}M_{\text{BH}}$ relation (e.g., Ferrarese & Merritt 2000; Gebhardt et al. 2000; Tremaine et al. 2002). Cumulative overdensities are summarized for several scales in Table 4.

We show that at scales $\lesssim 300 h_{70}^{-1}$ kpc, more massive black holes reside in environments more biased than those with lower mass. The relative bias is found by calculating the ratio of overdensity around the higher-mass black holes to the overdensity around the lower-mass black holes (lower panel of Figure 8). We find a linear fit ($y = AR + B$) to ratio values on all scales with parameters $A = -0.028$ and $B = 1.094$ (green line). This line also describes ratio values with $R \gtrsim 300 h_{70}^{-1}$ kpc (red line). However, points on scales $R \lesssim 300 h_{70}^{-1}$ kpc are better fit by a different line with parameters $A = -0.369$ and $B = 1.318$, which is shown in blue in the figure. To quantify the separation, we fit a line to the points $R \lesssim 300 h_{70}^{-1}$ kpc with slope $A = -0.028$ to match the best fit line to ratio values at all scales. The new line for ratio values $R \lesssim 300 h_{70}^{-1}$ kpc is 1.13 times higher than the line for all scales, a separation that has $> 3\sigma$ significance.

5. DISCUSSION

There are two main pictures through which observed differences in AGN can be interpreted. In the merger models presented by Hopkins et al. (2006), differing fueling mechanisms trigger AGN activity at different luminosities. Unified models such as those presented by Antonucci (1993) or Elvis (2000) ascribe observed differences in AGN to viewing angle or structure. We present definitive evidence that differences in *type* are caused by viewing angle or the internal structure of AGN, but differences in fueling mechanisms affect the *luminosity* of AGN. Our results in Figure 7 show that the clustering signature of Type II quasars on small scales is similar to the signature of bright Type I quasars. This suggests that the differences observed between Type I quasars and Type II quasars are due to orientation or internal structure effects. We conclude that Type II quasars are not a different

cosmological population from these bright quasars. There is a significant difference, however, in the environments of bright and Type II quasars and the environments of low-luminosity AGN, which implies that these populations have different fueling mechanisms. This result is consistent with results presented by Li et al. (2006, 2007), who find that there is only a weak link between near neighbors to narrow-line AGN and their nuclear activity.

We find that dim quasars with $-23.3 \leq M_i \leq -22.0$ are 1.12 times more overdense than the AGN sample ($>3\sigma$ significance) but 1.38 times less overdense than bright quasars with $-24.2 \leq M_i < -23.3$ ($>3\sigma$ significance). This suggests that the dim quasars are a transition population between low-luminosity AGN (likely fueled in dry mergers, close encounters, or secular processes) and high-luminosity AGN (likely fueled in major mergers). This could be evidence that rather than disparate populations of merger-fueled and secularly-fueled AGN, there is a continuum of galaxy interactions from major mergers to close encounters or harassment that cause AGN luminosity differences. Alternatively, a mix of mergers and secular processes could drive the AGN population near the quasar-Seyfert divide ($M_i \approx -22.5$; Hao et al. 2005).

We also show that more massive black holes reside in more biased environments on scales $\lesssim 300 h_{70}^{-1}$ kpc. Mergers with different merger mass ratios (e.g., Cox et al. 2007) can produce different black hole masses, and these various mergers will likely occur in environments with different densities. It is also possible that instead, or in combination with the differences in merger environments, post-merger events such as feedback (e.g., Wyithe & Loeb 2003; Di Matteo et al. 2005; Hopkins et al. 2005a) affect the local inter-galactic medium (IGM). If this feedback is correlated with the final black hole mass and stalled star formation in the local IGM, the local quasar environments could depend on black hole mass. The feedback occurring in mergers producing less massive black holes would have to suppress formation of galaxies near the quasar host galaxy on scales $\lesssim 300 h_{70}^{-1}$ kpc. Such a situation could occur if violent blowout phases not only ionize the local IGM to prevent star formation but also reduce the amount of available mass in the region of the central engine to be accreted onto the black hole.

In either case, our work suggests that pre-merger conditions for mergers that form quasars may be apparent in their post-merger environment. There is observational evidence for the merger origin of luminous quasars (e.g., Smith & Heckman 1989; Disney et al. 1995; Bahcall et al. 1997; Kirhakos et al. 1999; Guyon et al. 2006; Hutchings & Cherniawsky 2006; Urrutia et al. 2007), but this information typically has not shed light on the conditions that preceded the merger. Future simulations of the merger origin of quasars that include environment information both before and after the merger will have to reproduce our observed M_{BH} -environment relationship at $< 300 h_{70}^{-1}$ kpc.

6. CONCLUSIONS

Our work sheds new light on the nature of AGN environments and their relationship to physical properties of the AGN itself. We have used larger samples of AGN targets and imposed a photometric redshift cut on the nearby photometric galaxies to obtain overdensity estimates with more reliable errors for the local environments of AGN of various luminosities and types.

Type II quasars are shown to have a similar small-scale clustering signature to bright Type I quasars, which suggests that they are not a cosmologically different population. However, narrow-line AGN have a different clustering signature from quasars, implying that environment plays more of a role in quasar activity than for low-luminosity AGN.

Quasars with more massive black holes are known to form in more biased environments than those with lower mass black holes. We find, however, that this is especially significant at scales $\lesssim 300 h_{70}^{-1}$ kpc. We suggest that this bias enhancement may contain information about the environment conditions that preceded the formation of the quasar. Effectively, we have shown that there is an " $M_{\text{DMH}}-M_{\text{BH}}$ -scale" relation that models of quasar origin will have to reproduce.

We find that there is a small but significant redshift evolution of quasar overdensity on small scales for $z \leq 0.6$. This evolution was not evident in previous studies and requires further investigation in future work. Future work will also relate the physical properties of AGN to the types of galaxies in their environment.

Acknowledgements

We thank Will Serber and Ryan Scranton for helpful conversations.

RJB and ADM acknowledge support from Microsoft Research, the University of Illinois, and NASA through grants NNG06GH156 and NB 2006-02049. The authors made extensive use of the storage and computing facilities at the National Center for Supercomputing Applications and thank the technical staff for their assistance in enabling this work.

Funding for the creation and distribution of the SDSS Archive has been provided by the Alfred P. Sloan Foundation, the Participating Institutions, the National Aeronautics and Space Administration, the National Science Foundation, the U.S. Department of Energy, the Japanese Monbukagakusho, and the Max Planck Society. The SDSS Web site is <http://www.sdss.org/>.

The SDSS is managed by the Astrophysical Research Consortium (ARC) for the Participating Institutions. The Participating Institutions are The University of Chicago, Fermi-

lab, the Institute for Advanced Study, the Japan Participation Group, The Johns Hopkins University, the Korean Scientist Group, Los Alamos National Laboratory, the Max-Planck-Institute for Astronomy (MPIA), the Max-Planck-Institute for Astrophysics (MPA), New Mexico State University, University of Pittsburgh, University of Portsmouth, Princeton University, the United States Naval Observatory, and the University of Washington.

REFERENCES

Adelman-McCarthy, J. K. et al. 2007, *ApJS*, 172, 634

Antonucci, R. 1993, *ARA&A*, 31, 473

Bahcall, N. A. & Chokshi, A. 1991, *ApJ*, 308, L9

Bahcall, J. N., Schmidt, M., & Gunn, J. E. 1969, *AJ*, 157, L77

Bahcall, J. N. et al. 1997, *ApJ*, 479, 642

Barr, J. M. et al. 2003, *MNRAS*, 346, 229

Best, P.N. 2004, *MNRAS*, 351, 70

Blanton, M. et al. 2003, *ApJ*, 592, 819

Blanton, M. et al. 2007, *AJ*, 133, 734

Budavari, T. et al. 2003, *ApJ*, 595, 59

Coldwell, G. V. et al. 2002, *MNRAS*, 336, 207

Cox, T. J. et al. 2007, preprint (astro-ph/0709.3511v1)

Csabai, I. et al. 2003, *AJ*, 125, 580

da Angela, J. et al. 2007, preprint (astro-ph/0612401)

Di Matteo, T. et al. 2005, *Nature*, 433, 604

Disney, M. J. et al. 1995, *Nature*, 376, 150

Djorgovski, S. 1991 in *ASP Conf. Ser.* 21, *The Space Distribution of Quasars*, ed. D. Cramp-ton (San Francisco: ASP), 349

Djorgovski, S. et al. 2007, *ApJ*, 662, L1

Ellingson, E. et al. 1991, *ApJ*, 371, 49

Elvis, M. 2000, *ApJ*, 545, 63

Ferrarese, L. & Merritt, D. 2000, *ApJ*, 539, L9

Fisher, K. B. et al. 1996, *ApJ*, 468, 469

Gehardt, K. et al. 2000, *ApJ*, 539, L13

Guyon, O. et al. 2006, *ApJS*, 166, 89

Hao, L. et al. 2005, *AJ*, 129, 1795

Hennawi, J. et al. 2006, *AJ*, 131, 1

Hopkins, P. et al. 2005a, *ApJ*, 625, L71

Hopkins, P. et al. 2005b, *ApJ*, 630, 705

Hopkins, P. et al. 2006, *ApJS*, 163, 1

Hopkins, P. & Hernquist, L. 2006, *ApJS*, 166, 1

Hopkins, P. et al. 2007, *ApJ*, submitted (astro-ph/0706.1243v2)

Hutchings, J. B & Cherniawsky, A. 2006, *AJ*, 131, 680

Kirhakos, S. et al. 1999, *ApJ*, 520, 67

Kochanek, C. S. et al. 1999, *ApJ*, 510, 590

Kauffmann, G. et al. 2003, *MNRAS*, 346, 1055

Li, C. et al. 2006, *MNRAS*, 373, 457

Li, C. et al. 2007, preprint (astro-ph/0712.0883)

McLure, R. J. & J. S. Dunlop. 2001, *MNRAS*, 321, 515

Mortlock, D. J. et al. 1999, *MNRAS*, 309, 836

Myers, A., et al. 2007a, *ApJ*, 658, 99

Myers, A., et al. 2007b, preprint (astro-ph/0709.3474v1)

Porciani, C. & Norberg, P. 2006, *MNRAS*, 371, 1824

Schneider, D. P. et al. 2007, *AJ*, 134, 102

Serber, W. et al. 2006, *ApJ*, 643, 68

Smith, E. P. & Heckman, T. M. *ApJ*, 341, 658

Söchting, I. K. et al. 2004, *MNRAS*, 347, 1241

Tremaine, S. et al. 2002, *ApJ*, 574, 740

Urrutia, T. et al. 2007, preprint (astro-ph/0709.2805)

Wold, M. et al. 2001, *MNRAS*, 323, 231

Wurtz, R. et al. 2007, *ApJ*, 480, 547

Wyithe, J. S. B. & Loeb, A., 2003, *ApJ*, 595, 614

Yee, H. C. K. & Green, R. F. 1984, *ApJ*, 280, 79

Zakamska, N. et al. 2003, *AJ*, 126, 2125

Table 1. Mean cumulative overdensity of photometric galaxies around quasars and L^* galaxies for $z \leq 0.4$, with and without a photometric redshift cut on the photometric galaxy sample.

	$R_{max} (h_{70}^{-1} \text{ Mpc})$	$N_g(Q) / \langle N_g(R) \rangle$	$N_g(L^*) / \langle N_g(R) \rangle$	Ratio of Q to L^*
no δz	0.10	1.92 ± 0.056	1.24 ± 0.007	1.55 ± 0.046
	0.25	1.41 ± 0.022	1.14 ± 0.003	1.24 ± 0.020
	0.50	1.20 ± 0.012	1.10 ± 0.002	1.09 ± 0.011
	1.00	1.11 ± 0.007	1.06 ± 0.001	1.05 ± 0.007
	2.00	1.06 ± 0.005	1.04 ± 0.001	1.02 ± 0.005
$\delta z = 0.05$	0.10	3.20 ± 0.151	2.07 ± 0.024	1.55 ± 0.075
	0.25	2.06 ± 0.053	1.71 ± 0.010	1.20 ± 0.032
	0.50	1.55 ± 0.026	1.48 ± 0.005	1.05 ± 0.018
	1.00	1.30 ± 0.014	1.31 ± 0.003	0.99 ± 0.011
	2.00	1.17 ± 0.009	1.18 ± 0.002	0.99 ± 0.008

Table 2. Mean cumulative overdensity of photometric galaxies around quasars as a function of redshift.

Target	$R \lesssim 1.0 h_{70}^{-1} \text{ Mpc}$ Overdensity	$R \lesssim 140 h_{70}^{-1} \text{ kpc}$ Overdensity	$R \lesssim 100 h_{70}^{-1} \text{ kpc}$ Overdensity
Quasars $z \leq 0.4$	1.30 ± 0.0002	2.55 ± 0.008	3.07 ± 0.018
Quasars $0.4 < z \leq 0.6$	1.34 ± 0.0005	2.98 ± 0.033	3.43 ± 0.80

Table 3. Mean cumulative overdensity of photometric galaxies around different classes of AGN.

Target	δ_{Target}	$\delta_{Target}/\delta_{bright \ qso}$	$\delta_{Target}/\delta_{dim \ qso}$
$R \lesssim 1.0 \ h_{70}^{-1} \text{ Mpc}$			
Type II Quasars	1.44 ± 0.006	1.04 ± 0.005	1.11 ± 0.005
Bright Quasars ^a	1.37 ± 0.001
Dim Quasars ^b	1.30 ± 0.0002
AGN	$1.28 \pm 9.1 \times 10^{-6}$	0.949 ± 0.002	0.9925 ± 0.0002
$R \lesssim 140 \ h_{70}^{-1} \text{ kpc}$			
Type II Quasars	3.64 ± 0.356	0.96 ± 0.097	1.34 ± 0.132
Bright Quasars	3.47 ± 0.060
Dim Quasars	2.52 ± 0.007
AGN	2.11 ± 0.0002	0.637 ± 0.026	0.8793 ± 0.003
$R \lesssim 100 \ h_{70}^{-1} \text{ kpc}$			
Type II Quasars	5.03 ± 0.976	1.09 ± 0.217	1.57 ± 0.305
Bright Quasars	4.39 ± 0.154
Dim Quasars	2.97 ± 0.016
AGN	2.42 ± 0.0005	0.561 ± 0.045	0.859 ± 0.006

^a $-24.2 \leq M_i < -23.3$

^b $-23.3 \leq M_i \leq -22.0$

Table 4. Mean cumulative overdensity of photometric galaxies around quasars as a function of black hole mass.

Target	$R \lesssim 1.0 \ h_{70}^{-1} \text{ Mpc}$ Overdensity	$R \lesssim 140 \ h_{70}^{-1} \text{ kpc}$ Overdensity	$R \lesssim 100 \ h_{70}^{-1} \text{ kpc}$ Overdensity
Quasars $M_{BH} \leq 10^8 M_{\odot}$	1.26 ± 0.001	2.07 ± 0.034	2.48 ± 0.080
Quasars $M_{BH} \geq 10^{8.5} M_{\odot}$	1.32 ± 0.001	2.57 ± 0.041	2.90 ± 0.093

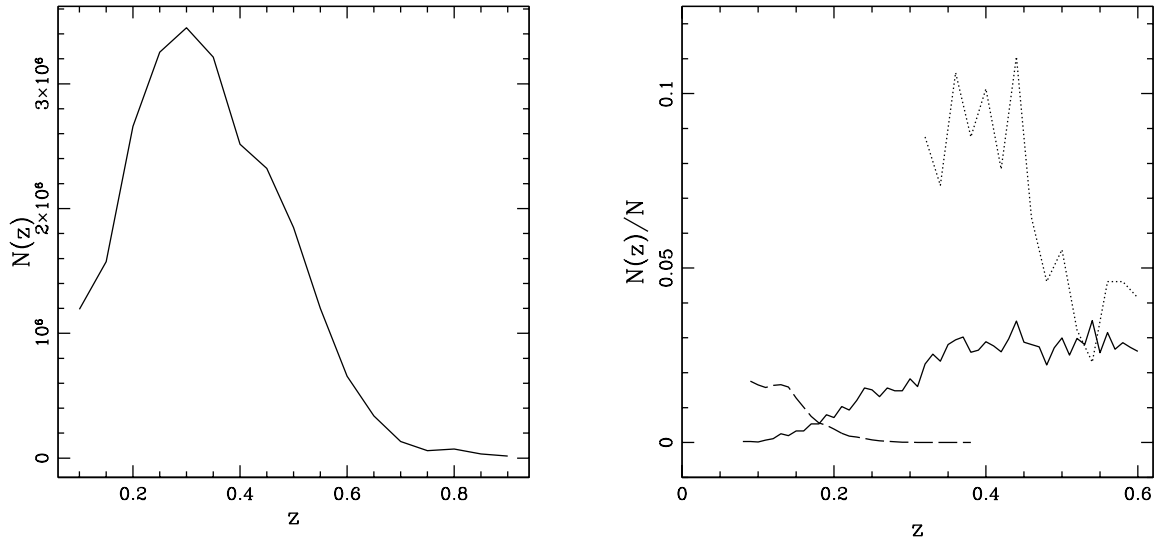


Fig. 1.— *Left*: Number of galaxies binned in redshift bins of $\delta z = 0.05$ based on their photometric redshifts from the SDSS DR5 Photoz Table with $14 \leq r \leq 21$ and satisfying flag cuts in the r -band. *Right*: Fractional number of targets binned in redshift bins based on their spectroscopic redshifts. The solid black line shows $N(z)/N_{QSO}$ for 7,549 spectroscopic quasars (Schneider et al. 2007), the dashed line shows $N(z)/N_{AGN}$ for 39,461 narrow-line AGN (Kauffmann et al. 2003), and the dotted line shows $N(z)/N_{TypeII}$ for 217 Type II quasars (Zakamska et al. 2003).

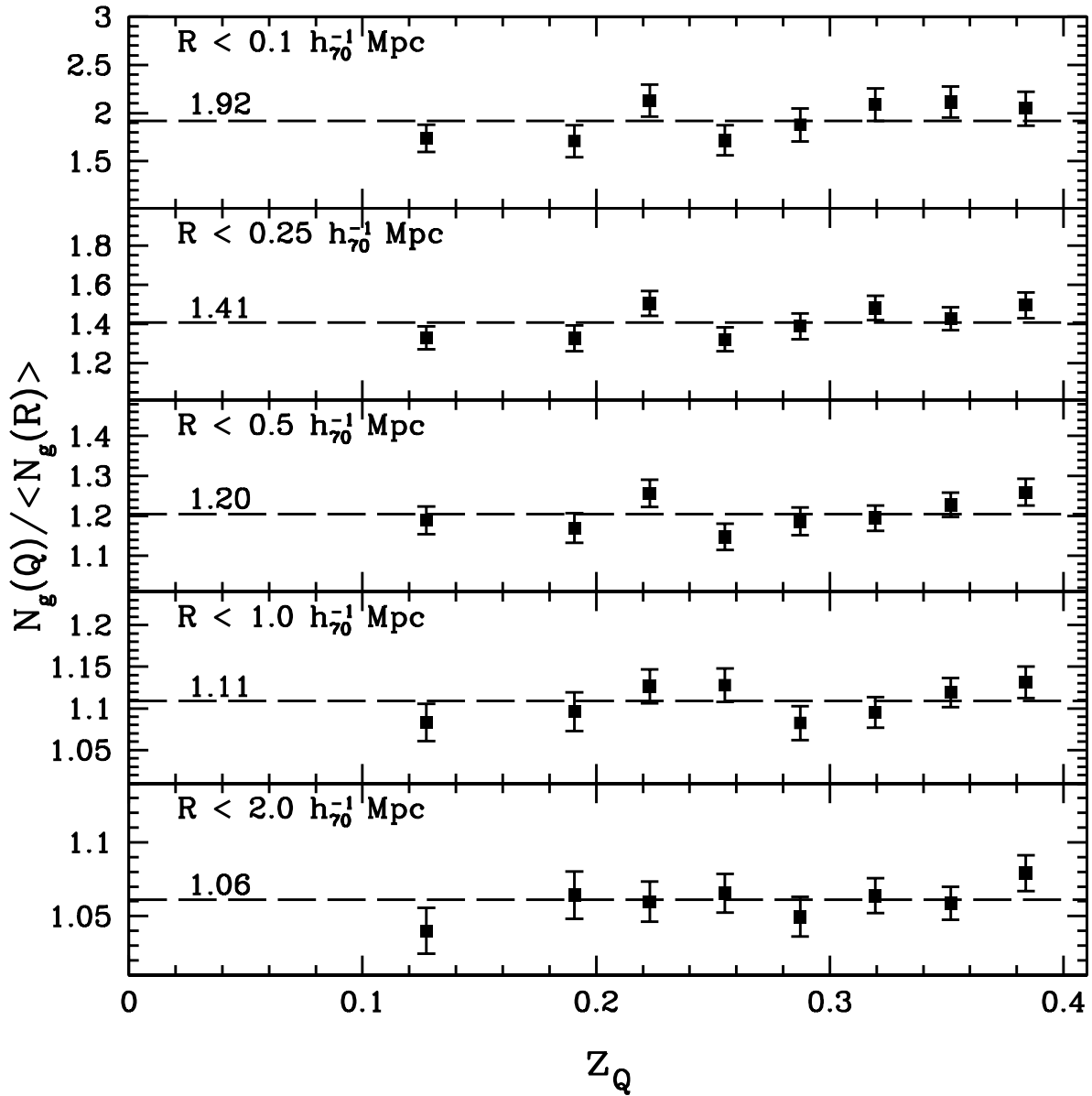


Fig. 2.— Mean cumulative overdensity of photometric galaxies with $14 \leq r \leq 21$ and satisfying flag cuts in the r -band around spectroscopic quasars as a function of redshift. The dashed line indicates the weighted mean overdensity in that radius bin.

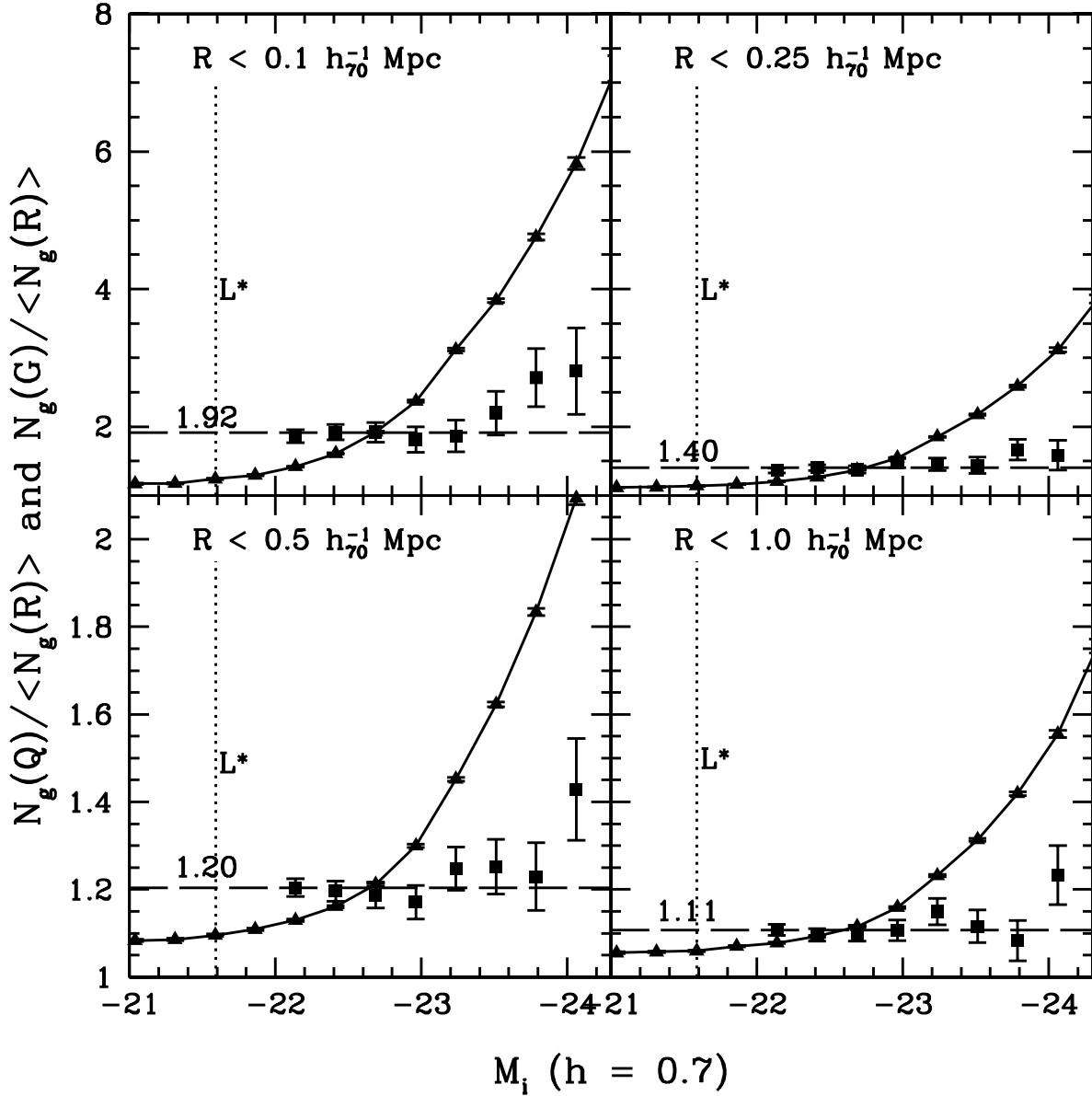


Fig. 3.— Mean cumulative overdensity of photometric galaxies with $14 \leq r \leq 21$ and satisfying flag cuts in the r -band around $z \leq 0.4$ spectroscopic quasars (solid squares) and galaxies (connected solid triangles) as a function of the targets' M_i . The horizontal dashed line indicates the weighted mean quasar overdensity in that radius bin for the $z \leq 0.4$ sample. The i -band L^* value of -21.59 (Blanton et al. 2003) is indicated by the vertical dotted line.

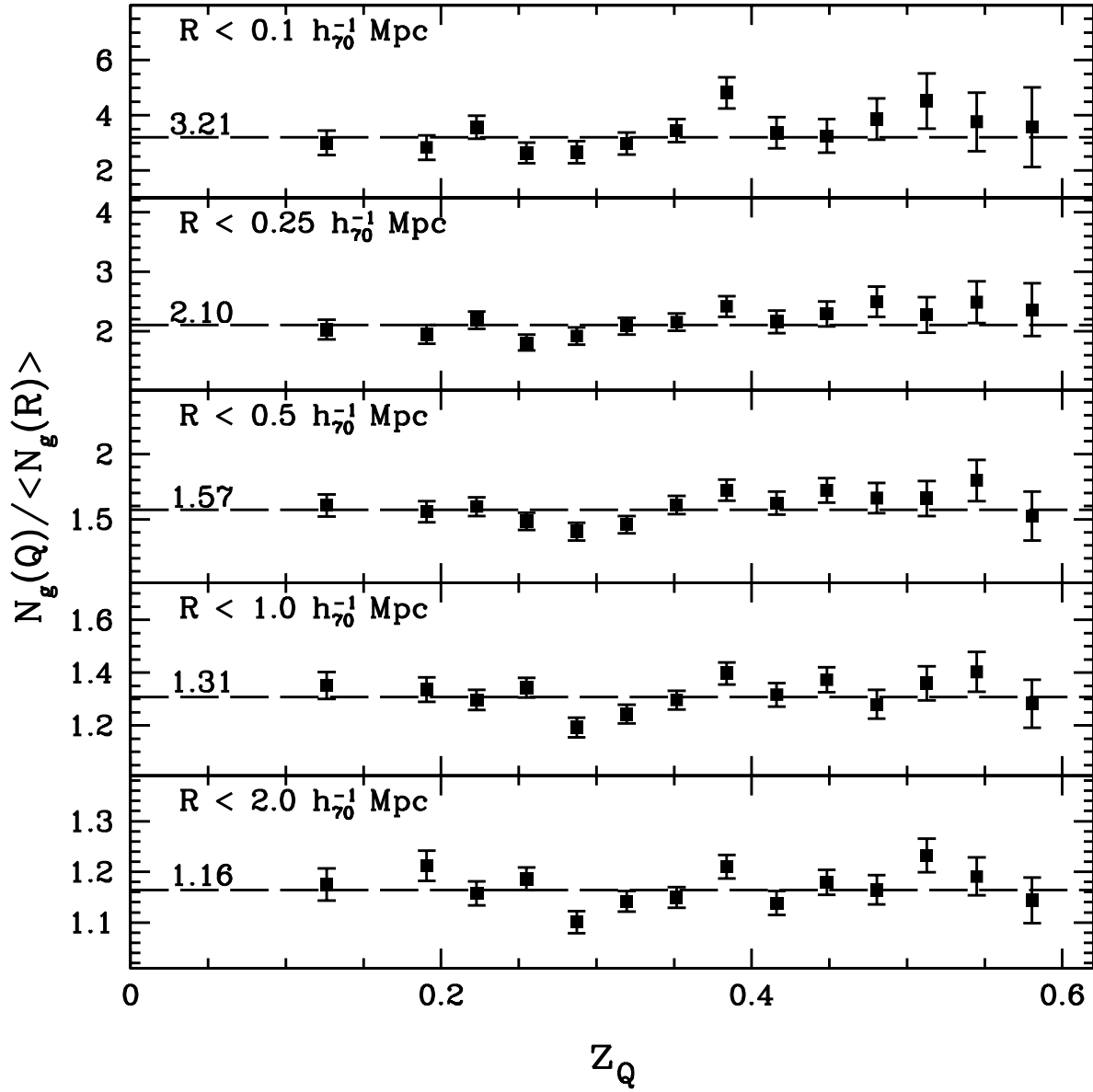


Fig. 4.— Same as Figure 2 but with a photometric redshift cut of $|z_{\text{target}} - z_{\text{photogal}}| \leq 0.05$ applied to the photometric galaxy sample.

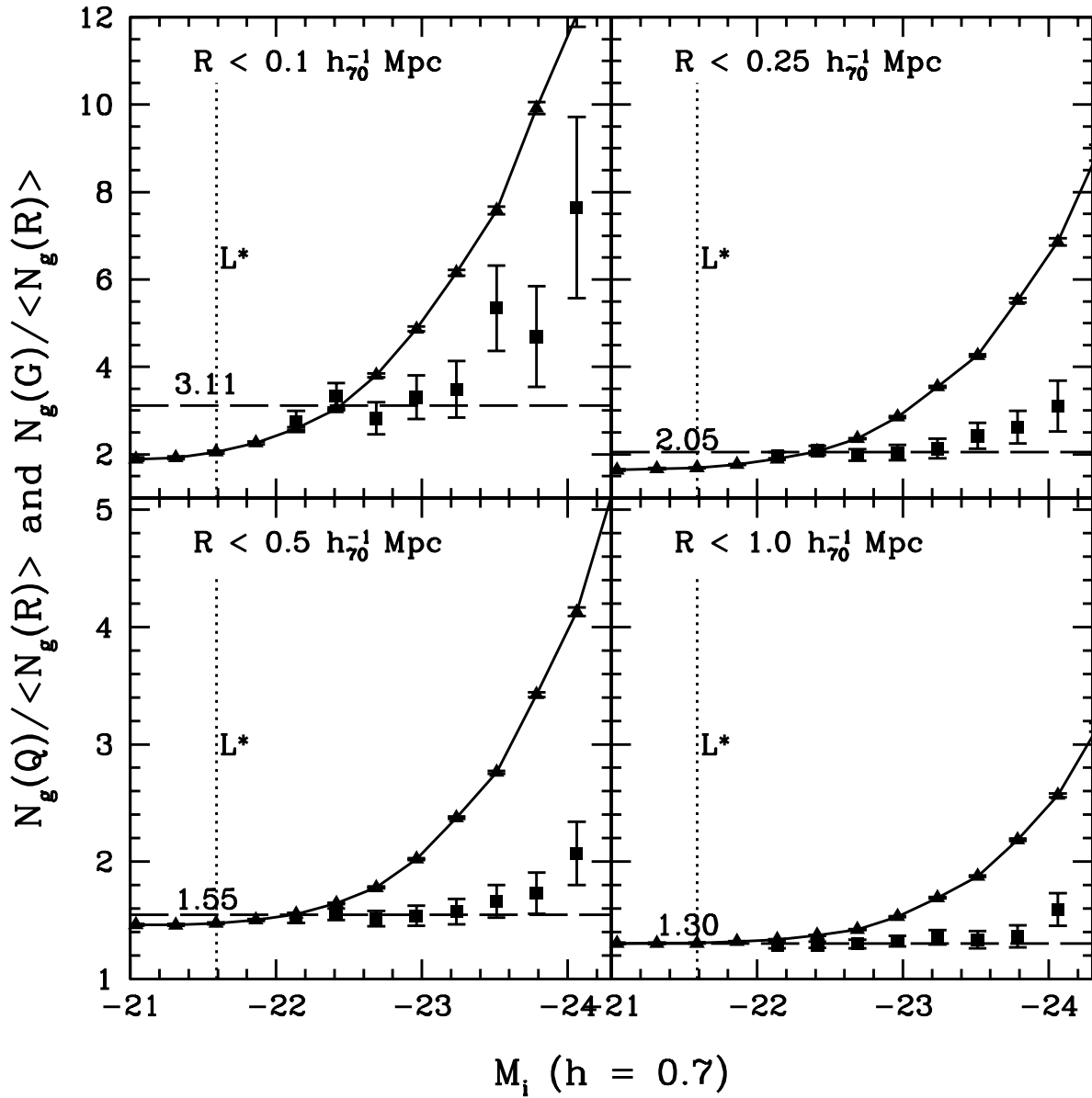


Fig. 5.— Same as Figure 3 but with a photometric redshift cut of $|z_{target} - z_{photogal}| \leq 0.05$ applied to the photometric galaxy sample.

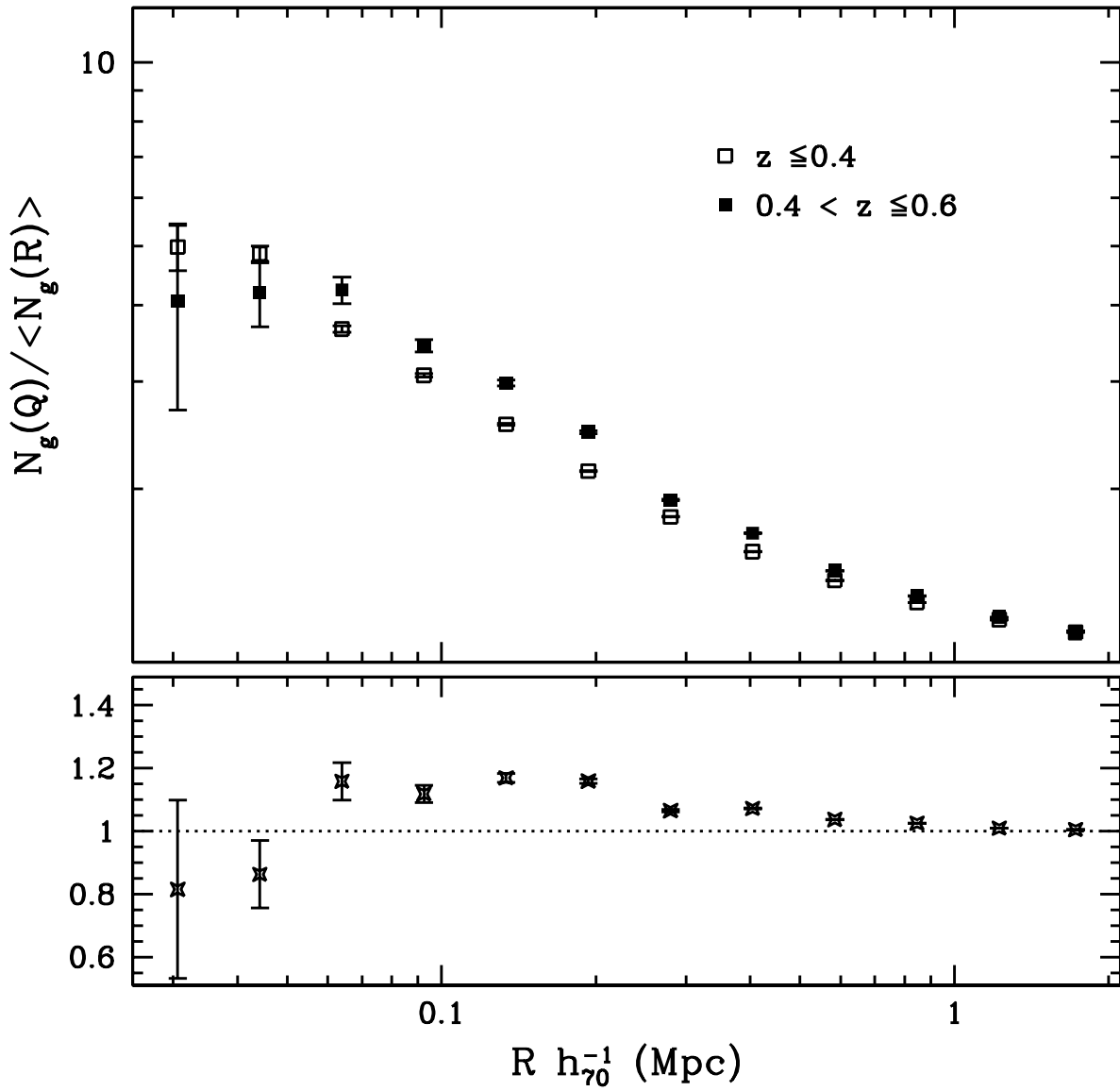


Fig. 6.— Mean cumulative overdensity of photometric galaxies around spectroscopic quasars with $z \leq 0.4$ (open black squares) and $0.4 < z \leq 0.6$ (solid black squares) as a function of comoving scale. The lower panel presents the overdensity ratio of high-redshift to low-redshift quasars.

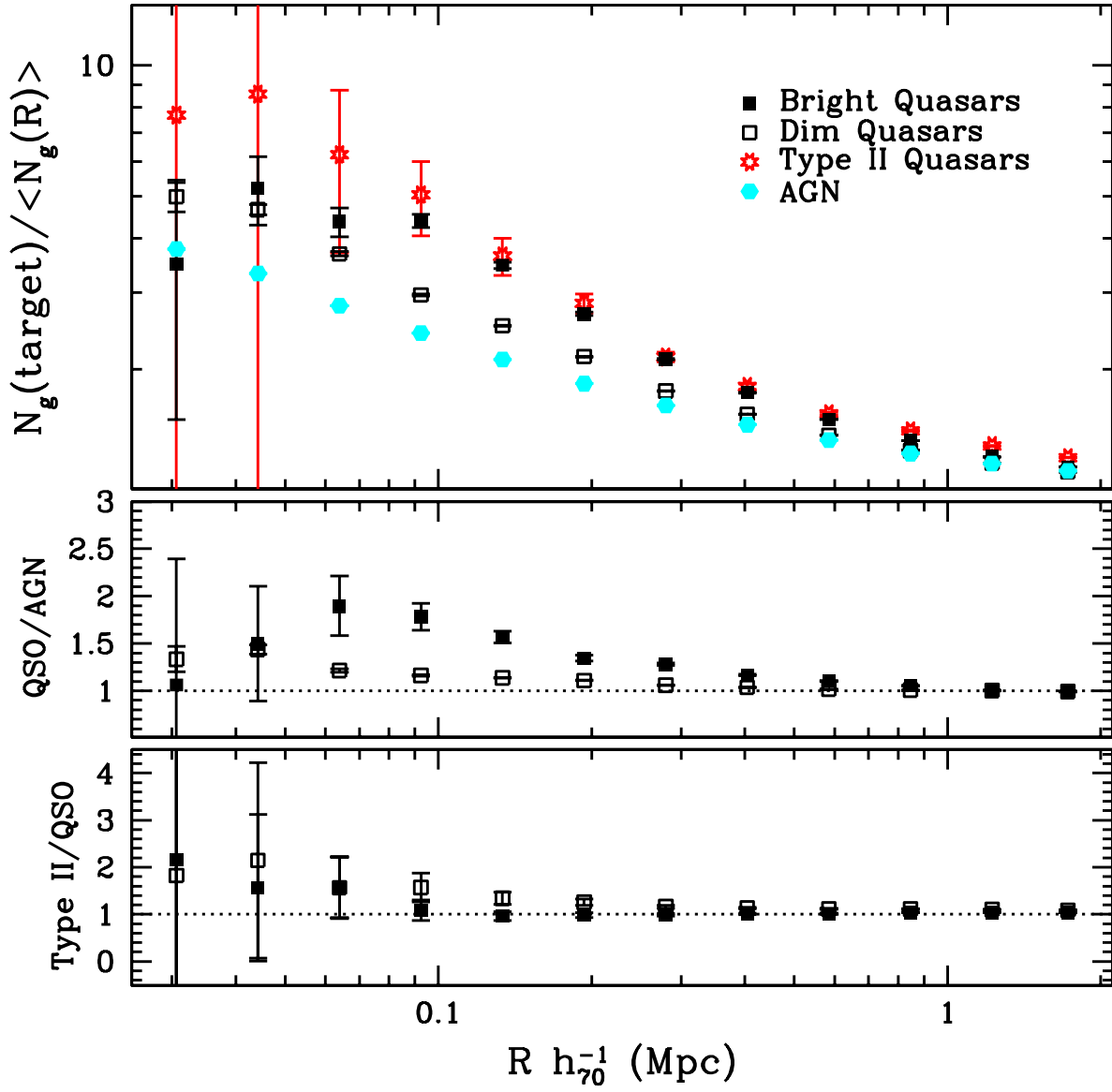


Fig. 7.— Mean cumulative overdensity of photometric galaxies as a function of comoving scale for two different quasar luminosity bins, Type II quasars (Zakamska et al. 2003), and narrow-line AGN (Kauffmann et al. 2003). Solid black squares represent bright quasars with $-24.2 \leq M_i < -23.3$, open green squares represent dim quasars with $-23.3 \leq M_i \leq -22.0$, open red starred points represent Type II quasars, and solid cyan hexagons represent narrow-line AGN. The middle panel shows the ratio of overdensities of bright (solid squares) and dim (open squares) quasars with $0.08 \leq z \leq 0.37$ to AGN. The lower panel shows the ratio of overdensities of Type II quasars to bright (solid squares) and dim (open squares) quasars with $0.3 \leq z \leq 0.6$.

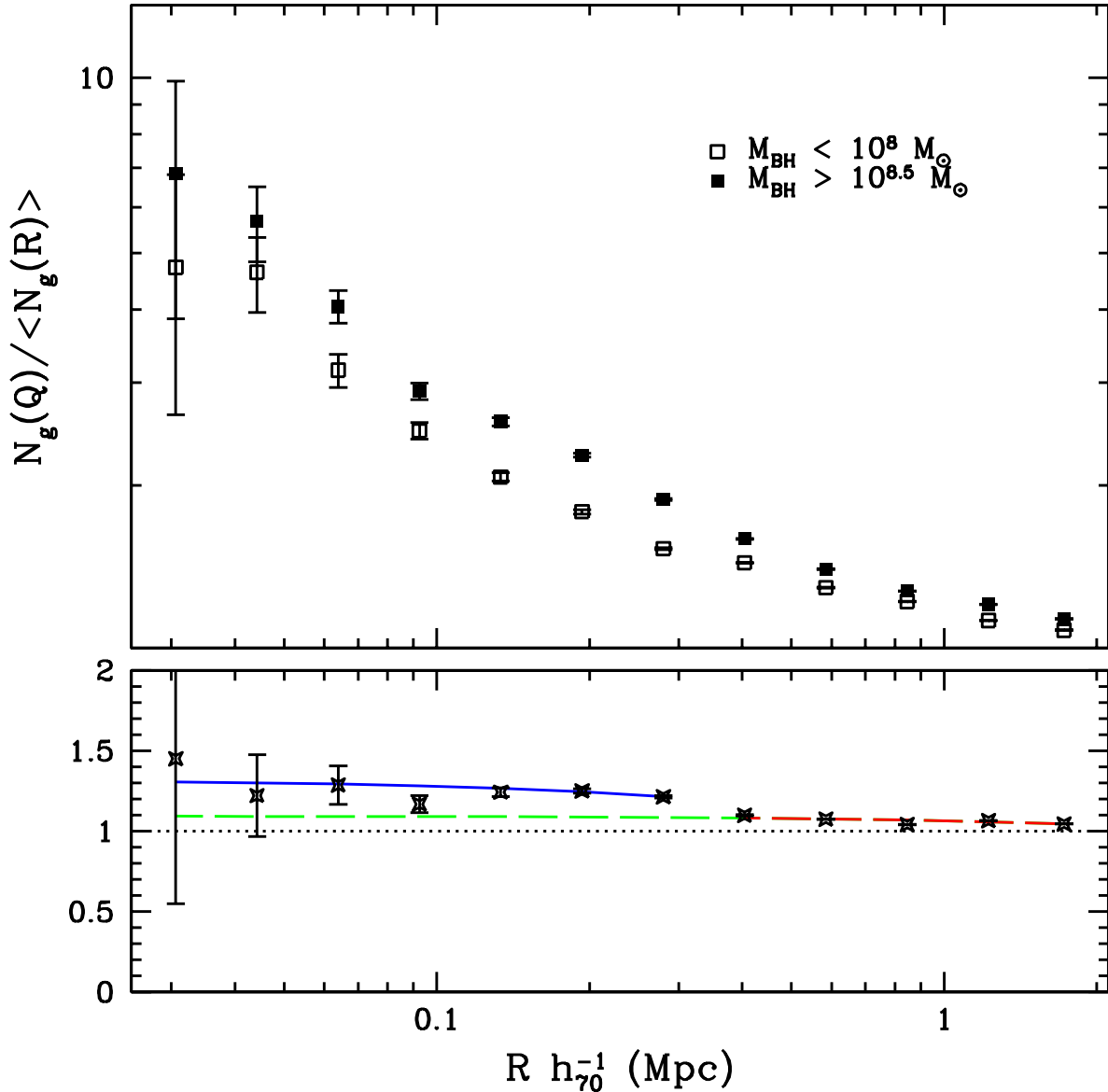


Fig. 8.— Mean cumulative overdensity of DR5 photometric galaxies around around $z \leq 0.4$ quasars as a function of comoving scale and black hole mass. Quasars with black hole mass $< 10^8 M_\odot$ are represented by open squares, and quasars with black hole mass $> 10^{8.5} M_\odot$ are represented by solid squares. The lower panel shows the ratio of overdensities around high-mass black holes to those around low-mass black holes. A linear fit ($y = -0.028R + 1.094$) to ratio values for $R \gtrsim 300 h_70^{-1}$ kpc is shown in red (dashed); this line is also the best fit to ratio values at all scales, which is shown in green (dashed). The blue line ($y = -0.369R + 1.318$) is the best linear fit to ratio values with $R \lesssim 300 h_70^{-1}$ kpc.